MEDWIN PUBLISHERS
Committed to Create Value for Researchers

Petroleum & Petrochemical Engineering Journal
ISSN: 2578-4846

# Prediction of Critical Drawdown Pressures for the Onset of Sand Production Using Conventional Triaxial Tests: A Case Study of Himmatnagar Sandstone

**Madem VK, Ghosh S and Balikram A***

Department of Petroleum Engineering, Indian Institute of Technology (ISM), India

***Corresponding author:** Archana Balikram, Department of Petroleum Engineering, Indian Institute of Technology (ISM), Dhanbad, Jharkhand, 826004, India

**Research Article**
**Volume 10 Issue 4**
**Received Date**: October 08, 2026
**Published Date:** November 12, 2026
DOI: 10.23880/ppej-16000420

## Abstract

Controlling damage from sand production in hydrocarbon-producing wells demands substantial capital investment. Therefore, our research focuses on sand-production tendency using geomechanical studies of sandstone cores to evaluate perforation stability. Eight samples of well sorted and uniform coarse-grained (CG) and fine-grained (FG) sandstone underwent uniaxial and triaxial tests for mechanical rock properties. Principal stresses at depth were chosen for three faulting regimes (i.e., normal, normal to strike-slip, strike-slip) and identical rock mechanical properties were considered at all depths. Safe minimum bottomhole flowing pressures ($SMP_{wf}$) for sand production onset and critical drawdown pressures (CDP) were calculated. Results indicate that at near-surface depths, perforating in either SHmax (maximum horizontal stress) or Shmin (minimum horizontal stress) direction will not result in sand production at high drawdowns ($SMP_{wf}$ < 0 for all samples). However, at depths > 1 km, the situation varies depending on the production drawdown, perforation orientation, and faulting regime. $SMP_{wf}$ is > 20 MPa at 2 km depth for most, if not all, cases. Perforation stability at depth is marginally to considerably higher (0-50 MPa difference in $SMP_{wf}$) when created in the SHmax, as opposed to Shmin direction. CG samples may witness the onset of sand production earlier than the FG samples due to their higher uniaxial compressive strengths (FG_UCS: 25.5 vs CG_UCS: 11.5 MPa). In all cases, for a given rock strength, sand production tendencies increase with perforation depth due to higher overburden and tectonic stresses. These observations assist operators in understanding sand production tendencies from rocks of similar mechanical properties located at various depths.

**Keywords:** Critical drawdown pressure; Perforation stability; Minimum flowing bottomhole pressure

## Introduction

Hydrocarbon-bearing rocks are susceptible to failure when subjected to abnormal forces that destabilize the porous rock geometry and ultimately lead to their breakage. Rock failure results in sand (fines) production along with reservoir fluids leading to severe damage to production equipment. Sanding is primarily triggered by three mechanisms, i.e., tensile failure, shear failure, and pore collapse [1]. Tensile failure of rock occurs under two circumstances. First, when the minimum effective stress on the rock exceeds its tensile strength. Second, when the effective radial stress is greater than or equal to the tensile limit of the rock [2]. Rock shear failure occurs when its strength is exceeded by in-situ shear stresses. Finally, pore collapse takes place when a critical level of effective stress is reached as a result of



CC BY

reservoir pressure depletion [1]. The interplay between in-situ stresses, drawdown, and fluid flow rate directly affects the material strength and determines which type of failure occurs [3].

Previous works extensively utilized conventional triaxial test apparatus to experimentally analyze the rock strength criteria and provide several conclusions on how rock failure affects the sand production phenomenon. For example, Kozhagulova, et al. [4], using laboratory experiments on weak sandstone analogs, mentioned that both applied stress levels and fluid flow rates significantly influenced sand production. Papamichos and Furui [5] devised analytical criteria for predicting sanding onset in the field, which are based on several parameters, such as simplified Mohr-Coulomb (modified critical stress), Mohr-Coulomb (critical stress), Von Mises (void ratio), and Drucker Prager (dilation potential) hole failure criteria to determine the critical formation strength, denoted as either the sand onset stress (σS) or uniaxial compressive strength (UCS), under specific in-situ conditions, drawdown, and depletion levels.

Reyes and Sipi [6] provided a detailed explanation of sand control design criteria, which enumerates the pre-implementation considerations, taking into account comprehensive rock mechanical studies, formation sand characterization, reservoir condition, lithological variations, production timeline, selection of appropriate gravel and stand-alone screen sizes, followed by completion method selection and economic evaluation. Apart from reservoir-related factors, sanding is intricately related to the drawdown pressure in a hydrocarbon-producing well. It requires advanced prediction methods and the knowledge of when and how to adjust the drawdown pressure that causes sanding [7]. Morita, et al. [3] observed that sand production increases at high flow rates, during sudden changes in flow rates, and with an increase in water cut.

Some researchers used hollow cylindrical samples to deduce the effects of external stresses and the rate of fluid flow on sand production over time [8]. According to the erosion-based criteria, sand production occurs when the forces due to drag from fluid flow exceed the apparent cohesion between the particles, as opposed to the shear (compressive) failure criterion that assumes sand production immediately follows material failure [1]. The process of erosion considers both pore fluid flow and the flow of solid particles. The rock's mechanical strength characteristics are crucial in determining its behavior before, during, and after the erosion process. Additionally, Yi, et al. [9] showed a dependence of rock collapse on the intermediate principal stress and hence, they incorporated the intermediate principal stress ( $\sigma_2$ ) as a parameter in their model.

Zoback [10] showed the effect of UCS on safe drawdown limits. In another study, Zoback [10] showed the effect of perforation orientation and well deviation on safe drawdown limits. Nemati, et al. [11] focused on the effects of reservoir pore pressure reduction on reservoir depletion. In such cases, maintaining similar production rates at different locations can cause variable sand production behavior. Papamichos and Malmanger [12] proposed a sand erosion model for estimating sand production with drawdown using field production history.

Even though the above-mentioned excellent studies address various facets of sand production, they did not address how different rocks with similar mechanical and reservoir properties occurring at various depths in the same well would behave in terms of sand production at different drawdowns. A similar scenario would be a single formation occurring at a range of depths. Tectonic events that result in uneven uplifting followed by erosion create circumstances where a reservoir quality formation forms hydrocarbon traps at various depths along laterally variable locations. In such cases, the mechanical properties of the formation may show little lateral variation, especially if the depositional environment is similar. It would be beneficial to investigate the differences in sand production behavior in these scenarios to provide operators with generalized guidance.

To theoretically address the effect of depth on sand production in such cases, we applied our uniaxial and triaxial mechanical core test results on drawdown equations provided by Masourizadeh. To generalize the results, we evaluated the suitability of multiple failure criteria, i.e., Mohr-Coulomb (M-C) criterion, Hoek-Brown (H-B), and Drucker-Prager (D-P), for the predictions. For further generalizations, calculations were carried out for three stress regimes, i.e., normal faulting, normal/strike-slip faulting, and strike-slip faulting. Finally, we also used two sandstones with different mechanical properties to understand any further variability in sand production. The lower limit of bottomhole flowing pressures ($SMP_{wf}$) followed by the critical drawdown pressure (CDP) calculations were performed using $SMP_{wf}$ equations for different relative stress magnitudes and chosen failure criteria. CDP estimation helps manage safe operating procedures for sand production [13]. This quantification of sanding onset, based on experimental rock mechanical studies and failure criteria, has the potential for applicability in a wide range of conditions, thereby making this work a unique addition to the body of literature on sand production tendency.

## Geological setting

The Himmatnagar sandstone core plugs were used in our study. This formation is primarily a horizontal to sub-



Copyright© Madem VK, et al.

horizontal formation and is exposed in flat-topped hillocks located east of Himmatnagar town (Gujarat, India). The stars depict the locations of the flat top outcrops for sample collection (Figure 1). Based on sedimentary structures, grain size variation, types of contacts, thickness of strata, vertical and lateral extension, and the presence of body (plant) and trace fossils, the depositional environment of the upper member of Himmatnagar sandstone formation is classified as fluvial to deltaic. The upper member displays trough cross-stratification, channel structures at the base, big wood fossils, angular to sub-rounded pebbles to cobbles in gritty sandstones [14]. The lower member has a marginal marine to marine depositional environment. Pancholi, et al. [15] reported a porosity range of 15-16% and a permeability of around 200 mD.

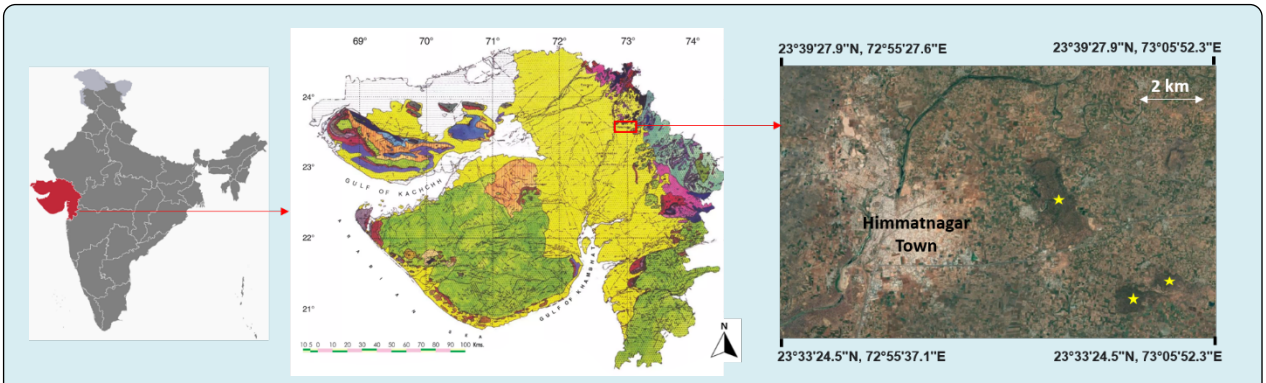



**Figure 1:** Location of Himmatnagar town and sandstone outcrops. Geological map obtained from GSMP [16].

## Methodology

A catalogue of the elements in the workflow followed in this study is provided in Figure 2. Broadly, these elements can be classified as sample preparation, experimental analyses, and findings & interpretations using existing mathematical models. The work begins with rock sample collection and ends with the estimation of the critical drawdown pressures.

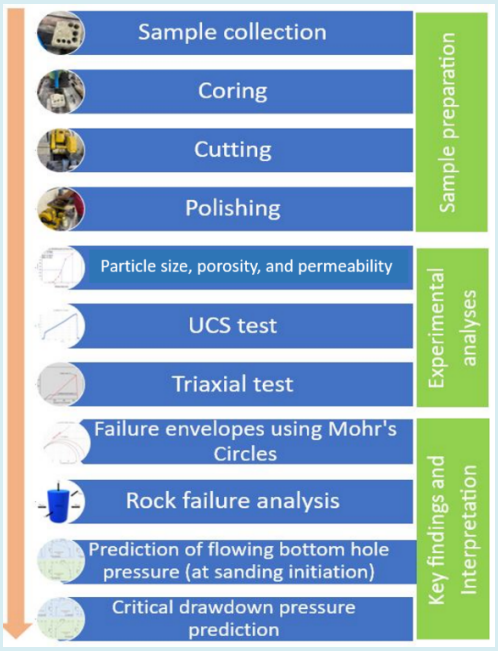



**Figure 2:** Workflow summary.

### Core Samples

The obtained rock blocks were cored using a standard coring machine (Figure 3). The core bit has an inner diameter of 55 inches and a length of about 1.3 ft. Water was used as the coring fluid. Thereafter, the obtained core plug samples were cut and polished. The retrieved core samples maintained a minimum L/D ratio of 2, as per the ASTM method of Triaxial Testing [17]. Figure 4 shows the eight core samples used in this study. Two types of sandstones, i.e., fine-grained and coarse-grained, were obtained.




**Figure 3:** Coring setup.



Copyright© Madem VK, et al.

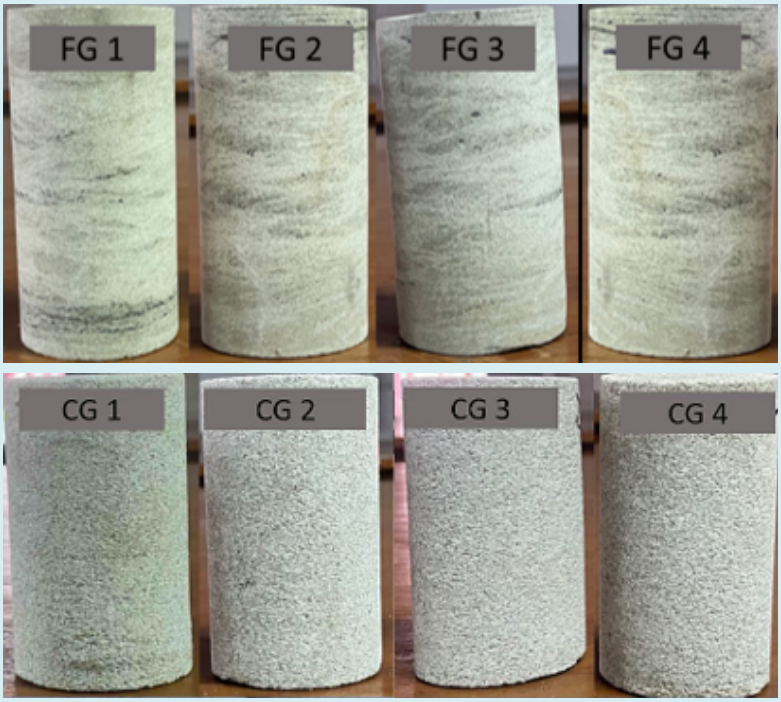



**Figure 4:** Fine-grained (FG 1-4) and core coarse-grained (CG 1-4) samples used in this study. Difference between the grain sizes is evident upon comparing the texture. One sample of FG and CG each was used for uniaxial tests and three samples each were used for triaxial tests.

### X-Ray Diffraction

For mineralogy, the Benchtop Smart Lab 9 kW instrument (Rigaku, Japan) was utilized to conduct X-ray diffraction (XRD) analysis on the powdered samples. This non-destructive testing method is useful in determining a material's physical characteristics, crystal structures, and composition of elements. Diffractograms (Intensity vs. 2θ angle plot) were produced, where each intensity peak corresponds to a specific mineral. The recognized peaks were qualitatively identified and elements were named.

### Particle Size Distribution, Porosity, and Permeability

The sieve analysis is a widely used procedure to obtain the particle size distribution of granular materials [18]. The particle size distribution plots were generated for both FG and CG samples using their loose rock masses According to ASTM D6913/D6913M-17 [19] standard. The porosities and permeabilities of the samples were also measured using a DCAM gas porosimeter/permeameter that uses Nitrogen gas.

### Uniaxial Compressive Strength (UCS) Test

According to ASTM D7012-23 [20] (Method C), the UCS test (Figure 5) is also called an unconfined compressive strength test which is used to find the strength of intact rock samples. In this test, the core specimen placed on the surface is loaded axially until its failure. This failure axial load is converted to the UCS of the sample using its cross-sectional area. This test was performed on two samples, one each for FG and CG plugs, namely FG4 and CG4.

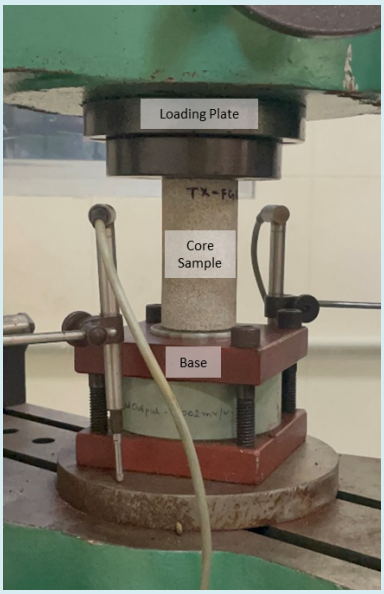



**Figure 5:** UCS test setup.



Copyright© Madem VK, et al.

### Triaxial Test

Laboratory triaxial tests are frequently employed to evaluate the mechanical properties of rock samples under specified conditions of confining stresses on rock core plugs. A schematic of the test setup is illustrated in Figure 6. In this test, a cylindrical rock sample enclosed in a membrane confined with fluid (applying a set confining stress) is subject to an axial compressive load. The resulting data on the stress-strain plot (acquired using CATMAN software) provides information on various rock mechanical properties, including its strength and elasticity.




**Figure 6:** Experimental setup for conventional triaxial testing.

As shown in Figure 6, the triaxial setup consists of (a) a confining fluid pump to provide confining pressure on the rubber membrane within which the sample is enclosed, (b) a triaxial cell with open top and bottom ends to apply axial load, (c) loading cell and a data collection system. Conventional triaxial tests were performed on coarse-grained core samples (CG1, CG2, CG3) with varying confining stresses of 1, 1.5, and 2 MPa and on fine-grained core samples (FG1, FG2, FG3) with varying confining stresses of 0.5, 1, and 1.5 MPa. Confining stresses between 0.5 - 2 MPa were chosen because at a higher confinement (i.e., > 2 MPa), the core samples did not fail at the machine's 200 bar maximum axial stress capacity. Applying an incremental 0.5 MPa confining stresses between each run separates the sample failure stresses at regular intervals allowing the creation of suitable failure envelopes.

During the tests, i.e., upon the application of the axial loads, the axial stresses were recorded continuously until the rocks failed (i.e., localized cracks were apparent). The axial loads were removed and samples were taken out and photographed for pre- and post-test comparisons. These are shown in the Results section.



Copyright© Madem VK, et al.

## Rock Failure Criteria

### Mohr-Coulomb (M-C) criterion

The M-C criterion is a classic rock failure criterion that dictates shear failure across a plane [21]. It has been used extensively to find the onset of sanding in petroleum reservoirs. Several researchers have proposed modifications to the M-C criterion to consider the effects of pore pressure, confining stress, and rock texture. This criterion relates shear stress to normal stress, cohesive strength, and tangent of friction angle as a linear equation (Equation 1) for several geomaterials, including rocks and consolidated soils.

$$\tau = S_0 + \sigma\, tan\left(\varphi_f\right) \quad (1)$$

where, τ = Shear stress (psi or MPa)
σ = Compressive stress (psi or MPa)
So= Cohesive strength (psi or MPa)
$\varphi_f$ = Internal friction angle (degrees)

The failure envelope is shown in Figure 7. In terms of principal stresses obtained from conventional triaxial tests, Equation 1 can be rewritten as:

$$\frac{\sigma_1 - \sigma_3}{2} = \frac{\sigma_1 + \sigma_3}{2}\sin\left(\varphi_f\right) + S_o\cos\left(\varphi_f\right) \quad (2)$$

where, $\sigma_1$ = Major principal stress (psi or MPa)
$\sigma_3$ = Minor principal stress (psi or MPa)

The advantage of this criterion is that it does not require the intermediate principal stress ($\sigma_2$), which is not measured by conventional triaxial test apparatus. However, non-consideration of the intermediate principal stress ($\sigma_2$) may also lead to the underestimation of material strength.

Upon rearranging Equation 2, the failure function is shown in Equation 3, as presented by Yi, et al. [9].

$$F = \left(\frac{\sigma_1 + \sigma_3}{2}\right)\sin\left(\varphi_f\right) + S_o\cos\left(\varphi_f\right) - \left(\frac{\sigma_1 - \sigma_3}{2}\right) \quad (3)$$

When F 0, failure of the body occurs

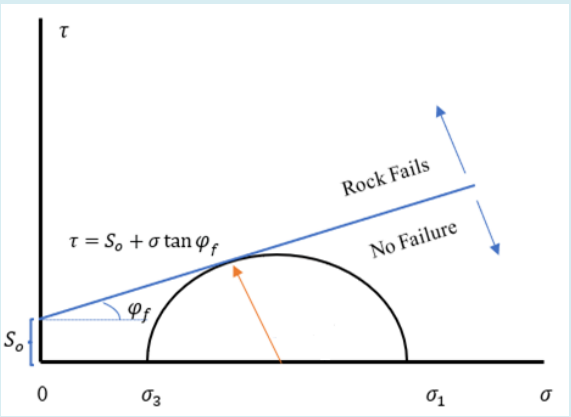



**Figure 7:** M-C failure envelope.

### Hoek-Brown (H-B) criterion

The H-B criterion [22] is another widely used rock failure criterion in the petroleum industry. It is a more sophisticated criterion that considers the effect of the rock type and the current state of deformation, in addition to rock strength, on its failure behavior. It is based on a modified M-C failure envelope that includes a non-linear term that reflects the rock's strength and deformation properties. The H-B criterion has been used to predict sand production in petroleum reservoirs. This criterion was established upon experiments in a wide variety of rocks, which involves two constants - 'm' and 's'. While 's' depends on the current state of deformation [23], 'm' depends on rock texture and mineralogy [24]. Equation 4 denotes the H-B criterion.

$$\frac{\sigma_1}{UCS} = \frac{\sigma_3}{UCS} + \sqrt{s + m\frac{\sigma_3}{UCS}} \quad (4)$$

Following Equation 4, failure function is given by Equation 5 as provided by Yi, et al. [9].

$$F = \frac{\sigma_1}{UCS} - \frac{\sigma_3}{UCS} - \sqrt{s + m\frac{\sigma_3}{UCS}} \quad (5)$$

| Lower Limit of 'm' | Upper Limit of 'm' | Rock Type | Examples |
|---|---|---|---|
| 5 | 8 | Carbonate rocks with good crystal cleavage | dolomite, limestone, marble |
| 4 | 10 | Argillaceous rocks | mudstone, shale, slate |
| 15 | 24 | Arenaceous rocks with strong and almost undeveloped crystal cleavage | sandstone, quartzite |
| 16 | 19 | Fine-grained polymineralic rocks | andesite, dolerite, diabase, rhyolite |
| 22 | 33 | Coarse-grained polymineralic rocks | amphibolite, gabbro, quartz-diorite |

**Table 1:** The values of 'm' for diverse rocks [10].



Copyright© Madem VK, et al.

Since the rock contains quartz as the dominant mineral, 'm' was chosen to be 20 (the average value of lower and upper limits for arenaceous rocks). Here, 's' was chosen as 1, assuming the rocks are intact (i.e., not naturally fractured or granulated).

**Drucker-Prager (D-P) criterion**

The D-P criterion [25] is widely used for modelling the failure behaviour of granular materials, including sand. This criterion is primarily a plasticity criterion that relates the material's shear strength to the pressure-dependent yield stress related to the fluid pore pressure and the mean stress. This criterion suggests that granular materials fail when the deviatoric stress surpasses a critical value determined by the friction angle, dilation angle, and cohesion. This criterion has been employed for predicting the onset of sand production in petroleum reservoirs. Different modifications have been proposed to consider the impacts of pore pressure and rock texture. Equation 6 shows the failure function as provided by Yi, et al. [9].

$$F = BI_1 + A - \sqrt{J_2} \quad (6)$$

where, $I_1 = \sigma_1 + \sigma_2 + \sigma_3$

$$J_2 = \frac{1}{6}\left[(\sigma_1 - \sigma_2)^2 + (\sigma_2 - \sigma_3)^2 + (\sigma_3 - \sigma_1)^2\right]$$

$$B = \frac{2\sin\varphi}{\sqrt{3}(3 - \sin\varphi)}$$

$$A = \frac{6S_o\cos\varphi}{\sqrt{3}(3 - \sin\varphi)}$$

where, $\sigma_2$ = Intermediate principal stress (psi). Other terms in the equations have been defined earlier in the text and also available in the Nomenclature section.

The rock is prone to failure when $F \le 0$.

**Comparison among the failure criteria**

Generally, true triaxial tests or polyaxial tests are better suited to predict the sanding tendency compared to conventional triaxial tests, which only use the major and minor principal stresses. The M-C and H-B criteria utilize $\sigma_1$ and $\sigma_3$ for the calculation of failure functions. Whereas, D-P criterion requires $\sigma_2$ which is obtained only from true triaxial tests. In conventional triaxial tests, which is a Kármán-type triaxial test, the intermediate and minor principal stresses are equal i.e., $\sigma_2 = \sigma_3$ [26]. Since there is no provision to measure intermediate principal stress ($\sigma_2$) to predict the failure function from D-P criteria in this work, we have treated $\sigma_2$ and $\sigma_3$ as equals.

## Kirsch Equations

The Kirsch equations [27] provide a means to calculate the radial, tangential, vertical stress values (Equation 7, 8, 9) in a cylindrical coordinate system, i.e., around a vertical well of radius 'R' in an isotropic, elastic medium.

$$\sigma_r = \frac{1}{2}(S_{H\,max} + S_{H\,min})\left(1 - \frac{R^2}{r^2}\right) + \frac{1}{2}(S_{H\,max} - S_{hmin})\left(1 - 4\frac{R^2}{r^2} + 3\frac{R^4}{r^4}\right) cos2\theta \quad (7)$$

$$\sigma_\theta = \frac{1}{2}(S_{H\,max} + S_{H\,min})\left(1 + \frac{R^2}{r^2}\right) - \frac{1}{2}(S_{H\,max} - S_{hmin})\left(1 + 3\frac{R^4}{r^4}\right) cos2\theta \quad (8)$$

$$\sigma_z = S_v - 2v\left(S_{H\,max} - S_{hmin}\right)\left(\frac{R^2}{r^2}\right)\cos 2\theta \quad (9)$$

where, $\sigma_r$ = Radial stress (MPa)

$\sigma_\theta$ = Tangential stress (MPa)

$\sigma_z$ = Axial stress (MPa)

$S_v$ = Vertical overburden stress (MPa)

r = Distance of any arbitrary point around the wellbore measured from wellbore axis (m)

$S_{H\,max}$ = Maximum horizontal stress (MPa)

$S_{hmin}$ = Minimum horizontal stress (MPa)

R= Radius of the wellbore (m)

θ = Angle measured from the azimuth of

v = Poisson's ratio

The radial, tangential, and vertical stress values were used as inputs in calculating the flowing bottomhole pressure in later sections of this work. Also, the calculation of Sv, SHmax, and Shmin values are shown in the upcoming sections.

## Prediction of the Onset of Sand Production

We quantitatively determined the sand production onset flowing bottomhole pressure ($SMP_{wf}$), which is the Pwf below which sand production occurs [23]. The M-C and H-B criteria for $SMP_{wf}$ are discussed. As mentioned later, the D-P criterion did not predict the observed core plug sample failure from the triaxial tests at the test conditions. Therefore, it was discarded for $SMP_{wf}$ predictions.

**Sand production threshold according to M-C criterion**

The $SMP_{wf}$ expressions for M-C criterion are shown in Table 2. The flowing bottomhole pressure (Pwf) below which sand production occurs depends on the relative principal stress magnitudes in the wellbore coordinate system.



Copyright© Madem VK, et al.

| No. | Stress State | Flowing bottomhole pressure (Mansourizadeh et al. 2016) |
|---|---|---|
| 1 | $\sigma_z \geq \sigma_\theta \geq \sigma_r$ | $SMP_{wf} = \frac{\left[S_v + 2v\left(S_{H\max} - S_{h\min}\right) - UCS\left(P_p\left(q-1\right)\right)\right]}{q}$ |
| 2 | $\sigma_z \geq \sigma_\theta \geq \sigma_r$ | $SMP_{wf} = \frac{\left[\left(3S_{H\max} - S_{h\min}\right) - UCS\left(P_p\left(q-1\right)\right)\right]}{1+q}$ |
| 3 | $\sigma_\theta \geq \sigma_r \geq \sigma_z$ | $SMP_{wf} = 3S_{H\max} - S_{h\min} - \left(UCS - P_p\left(q-1\right)\right) - q\left(S_v + 2v\left(S_{H\max} - S_{h\min}\right)\right)$ |

**Table 2:** Safe flowing bottomhole pressures ($SMP_{wf}$) below which sand production occurs as per the M-C criterion.

where, $P_p$ = Pore pressure (MPa)

Here, q is an empirical parameter that depends on friction angle [23] and written as:

$$q = \frac{1+\sin\varphi_f}{1-\sin\varphi_f} \quad (10)$$

**Sand production threshold according to Hoek-Brown criterion**

The H-B criterion is a non-linear, empirical (2 dimensional) criterion [28]. The $SMP_{wf}$ expressions for H-B criterion are shown in Table 3.

| No. | Stress State | Flowing bottomhole pressure [23] |
|---|---|---|
| 1 | $\sigma_z \geq \sigma_\theta \geq \sigma_r$ | $SMP_{wf} = 0.5\left(m\left(UCS\right)+2A\right) - \sqrt{\left(2A+m\left(UCS\right)\right)^2 - 4\left(A^2 + m\left(UCS\right)P_p\right) - s\left(UCS\right)^2}$ |
| 2 | $\sigma_\theta \geq \sigma_z \geq \sigma_r$ | $SMP_{wf} = \frac{1}{8}\left[\left(4D+m*UCS\right) - \sqrt{\left(4D+m*UCS\right)^2 - 16\left(D^2 + m\left(UCS\right)P_p\right) - s*UCS^2}\right]$ |
| 3 | $\sigma_\theta \geq \sigma_r \geq \sigma_z$ | $SMP_{wf} = 0.5\left[2\left(D-A\right) - \sqrt{4\left(D-A\right)^2 - 4\left(\left(D-A\right)^2 - s(UCS)^2 - m*UCS\left(A-P_p\right)\right)}\right]$ |

**Table 3:** $SMP_{wf}$ below which sand production occurs as per the H-B criterion.

where, A and D are given by:

$$A = \sigma_v + 2v\left(S_{H\max} - S_{h\min}\right)$$

$$D = 3S_{H\max} - S_{h\min}$$

## Stress Calculations

Application of the failure models to the subsurface requires principal stress values at depth. Calculation depth 147 m (482 ft) was chosen based on confining stress of 2 MPa (290 psi), which is the highest lateral stress experienced by the sample during the triaxial tests (i.e., 0.5, 1, 1.5, and 2 MPa). At the subsurface depth of 147 m (482 ft), 290 psi confining stress is reasonable, assuming a minimum horizontal stress gradient of 0.6 psi/ft or 0.6*Sv (assuming a Sv gradient of 1 psi/ft). The lower bound on Shmin is approximately 0.6*Sv [10, p. 12]. This value is reasonable considering a crustal friction coefficient of ~0.67.

Two more depths were calculated such that the arbitrarily chosen minimum horizontal stresses (Shmin) in the subsurface would be nearly 2000 psi (13.79 MPa) and 4000 psi (27.58 MPa) based on Sv gradient of 1 psi/ft and Shmin gradient of 0.6 psi/ft. These depth values were calculated as 1016 m and 2032 m, which are reasonable numbers considering oil production. To increase the data density, we included additional depths of 250 m, 500 m, 750 m, 1250 m, 1750 m, 2250 m, 2500 m, 2750 m, and 3000 m, resulting in 12 depth points for $SMP_{wf}$ and CDP calculations. Based on the statistic that most of the world's oil production happens in normal and strike-slip faulting regimes, we chose normal faulting (NF), normal to strike-slip (NF-SS), and strike-slip (SS) regimes for sand production thresholds ($SMP_{wf}$). Sv was calculated based on the aforementioned depths. Thereafter, Anderson's scheme [29] was used to identify the possible relative magnitudes of SHmax and Shmin at the aforementioned depths for the three mentioned stress regimes, assuming a crustal friction coefficient of ~0.67. Depending upon the faulting regime, pre-existing faults in the earth's crust impose limits on the relative magnitudes of the three principal stresses [10].



Copyright© Madem VK, et al.

Table 4 shows the chosen gradients for principal stresses according to the stress regimes considered for calculating $SMP_{wf}$ values. In the NF-SS regime, SHmax and Sv have similar gradients and Shmin is lower. However, in the case of the NF regime, SHmax falls between Sv and Shmin. In the SS regime, SHmax is greater than both Shmin and Sv, with a pore pressure gradient set at 0.44 psi/ft. (i.e., normal pore pressure).

| Stress Regime | Gradients (psi/ft) | | | |
|---|---|---|---|---|
| | $P_{p,g}$ | $S_{hmin,g}$ | $S_{Hmax.g}$ | $S_{V,g}$ |
| Normal faulting (NF) ($S_{Hmax}$ halfway between $S_{hmin}$ and $S_v$) | 0.44 | 0.6 | 0.85 | 1 |
| Normal to strike-slip (NF-SS) ($S_{Hmax} = S_V > S_{hmin}$) | 0.44 | 0.6 | 1 | 1 |
| Strike-slip (SS) faulting ($S_{Hmax} > S_V > S_{hmin}$) | 0.44 | 0.75 | 1.5 | 1 |

**Table 4:** Chosen gradients for principal stress calculations in different stress regimes.

## Results

### X-Ray Diffraction

XRD is a reliable technique, widely used in determining mineralogy of crystalline rocks. It depicts the diffraction intensities and corresponding peak positions. Pattern matching of intensity vs. diffraction angle of known minerals with those of test samples helps in the identification and quantification of minerals in the test sample. Other techniques that may be used for mineralogy estimation are Fourier transform infrared spectroscopy (FTIR) and energy dispersive spectroscopy (EDS). In this study, the XRD technique was used due to its ready availability.

XRD spectrum of FG and CG samples, respectively, are shown in Figure 8. From the XRD analysis, it is evident that quartz is dominant (> 95%) with highest intensity in both rock types. In the FG samples, minor amounts of muscovite (3%) and other trace minerals were identified. In the CG samples, along with quartz, minor amounts of dolomite (3%) and siderite (1%) were identified. Lattice plane information is also shown in the plots.

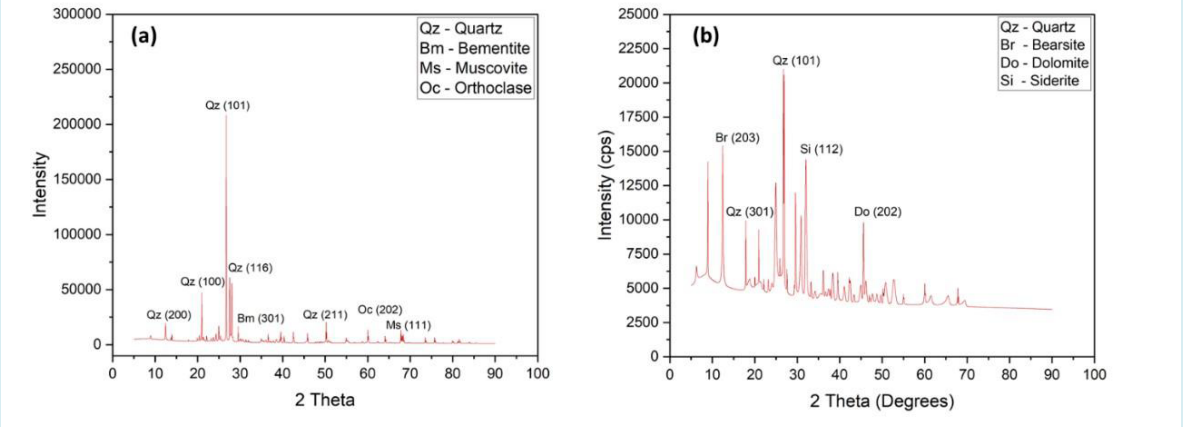



**Figure 8:** XRD Analysis of (a) FG sample and (b) CG sample.

### Particle Size Distribution, Porosity, and Permeability

Particle size distribution analysis of both FG and CG samples are shown in Figure 9. As observed from the plot, the average grain size (D50) of coarse-grained samples is 0.4 mm while that of fine-grained samples is 0.1 mm. The calculated values of the uniformity coefficient of coarse-grained and fine-grained samples are shown in Table 5. Equation 11 and 12 denote the formulae to calculate uniformity coefficient (UC) and sorting coefficient (SC), as provided by Bhattacharyya and Das [30].



Copyright© Madem VK, et al.

$$UC = \frac{D_{40}}{D_{90}} \quad (11)$$

$$SC = \frac{D_{10}}{D_{95}} \quad (12)$$

where, D10 = 10th percentile grain diameter
D40 = 40th percentile grain diameter
D90 = 90th percentile grain diameter
D95 = 95th percentile grain diameter (i.e., only 5% grains have diameter greater than D95)

| | Uniformity coefficient | Sorting coefficient | Porosity (%) | Permeability (mD) |
|---|---|---|---|---|
| Coarse-grained (CG) sample | 0.152 | 0.016 | 21.8 | 92 |
| Fine-grained (FG) sample | 0.03 | 0.04 | 24.5 | 1425 |

**Table 5:** Uniformity coefficient, sorting coefficients, porosity, and permeability of tested samples.

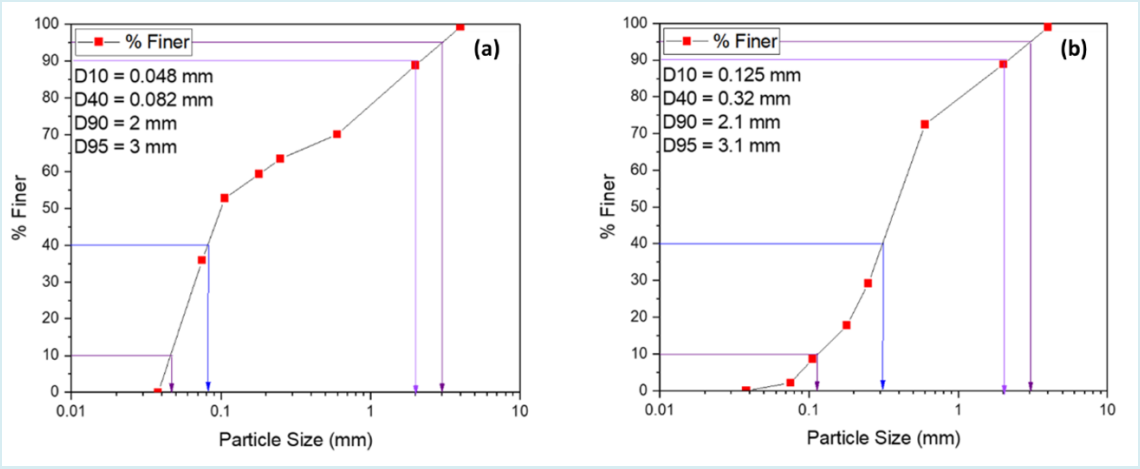



**Figure 9:** Particle size distribution plots of (a) fine-grained and (b) coarse-grained samples.

Based on a study by Friedman [31], for sandstones both CG and FG samples may be categorized as well sorted (SC < 2.5). Also, according to Reyes and Sipi [6], sand in both the samples may be classified as highly uniform (UC < 3), as observed from Table 6. Uniform grains distribute rock stress more evenly, leading to lower chances of grain crushing. Shahsavari and Shakiba [32] mentioned that larger the grain size range, lower the porosity and permeability. Therefore, well sorted sandstones with uniform grains result in high quality reservoirs with superior flow qualities and are favorable for oil and gas production.

Both FG and CG samples exhibit high porosity and permeability, as indicated by the average values in Table 5. This can be attributed to their high uniformity and sorting. Surprisingly, the FG sample demonstrated the higher porosity and permeability, a finding confirmed through repeated tests on both the same and different intact samples, with no visible fractures.

| Uniformity Coefficient | Classification |
|---|---|
| UC ≤ 3 | Sand is highly uniform |
| 3 ≤ UC ≤ 5 | Sand is uniform |
| 5 ≤ UC ≤ 10 | Sand is reasonably uniform |
| UC ≥ 10 | Sand is non-uniform |

**Table 6:** Sand particle uniformity classification (Reyes and Sipi 2018).

## Failure Analysis of the Samples Before and After Test

Upon carrying out the triaxial test of FG samples at relatively low confining stress (0.5 MPa), the samples suffered a total collapse, i.e., multiple catastrophic fractures (Figure 10). On the other hand, at relatively high confining stresses (1 and 1.5 MPa), FG samples witnessed only one or two faint tensile failure planes oriented parallel to the



Copyright© Madem VK, et al.

sample axis (Figures 11 and 12). The CG samples witnessed more than one shear failure plane at a low confining stress of 1 MPa (Figure 13). CG samples at medium (1.5 MPa) to high (2 MPa) confining stresses witnessed single major shear failure planes oriented 20o-30o with respect to the sample axis (Figuress 14 and 15 respectively).




**Figure 10:** FG 1 sample (a) before and (b) after failure at 0.5 MPa confining stress.

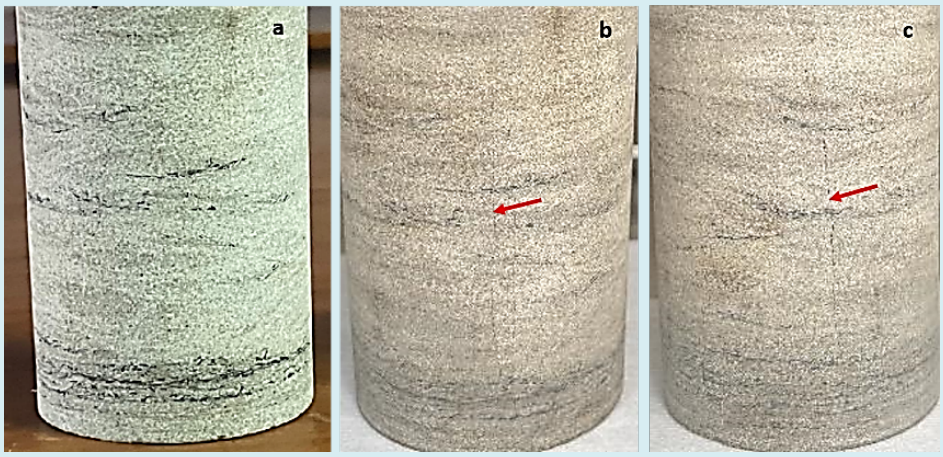



**Figure 11:** FG 2 sample (a) before and (b, c) after failure at 1 MPa confining stress.

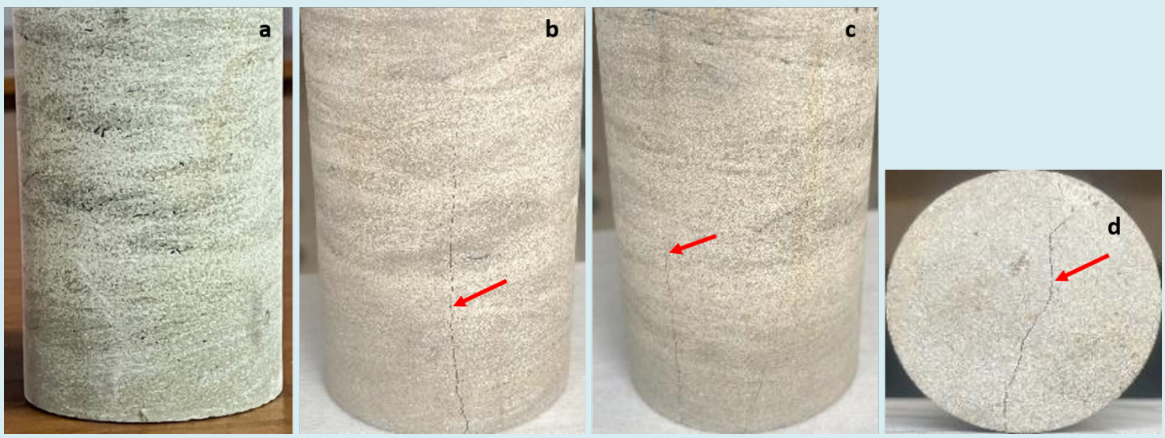



**Figure 12:** FG 3 sample (a) before and (b, c, d) after failure at 1.5 MPa confining stress.



Copyright© Madem VK, et al.

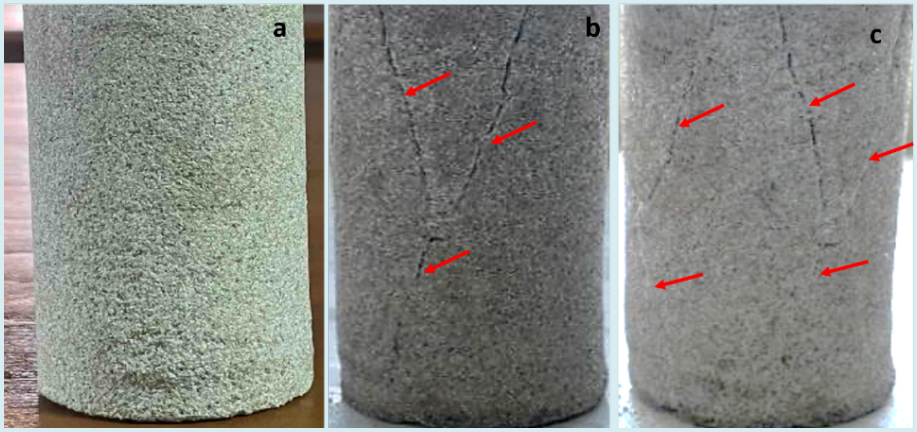



**Figure 13:** CG1 sample (a) before and (b, c) after failure at 1 MPa confining stress.

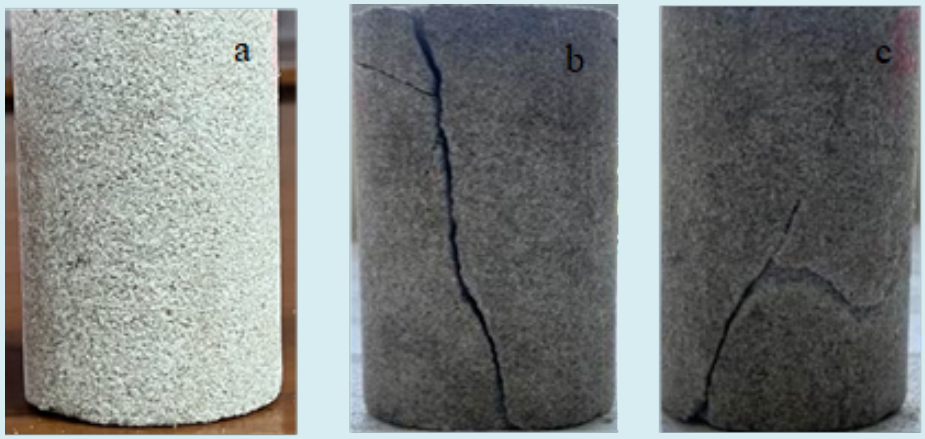



**Figure 14:** CG2 sample (a) before and (b, c) after failure at 1.5 MPa confining stress.

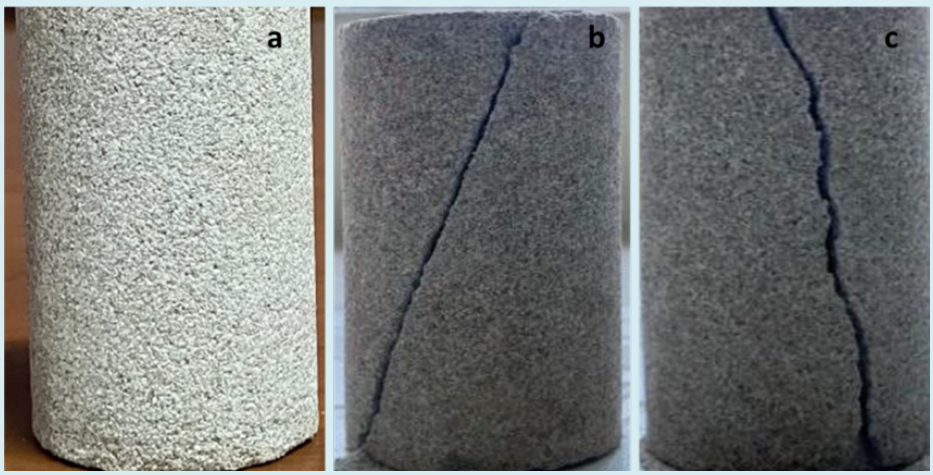



**Figure 15:** CG3 sample (a) before and (b, c) after failure at 2 MPa confining stress.



Copyright© Madem VK, et al.

The linear fits between axial load and confining stress (R2 > 0.97 for both CG and FG samples) are shown in Figure 16.

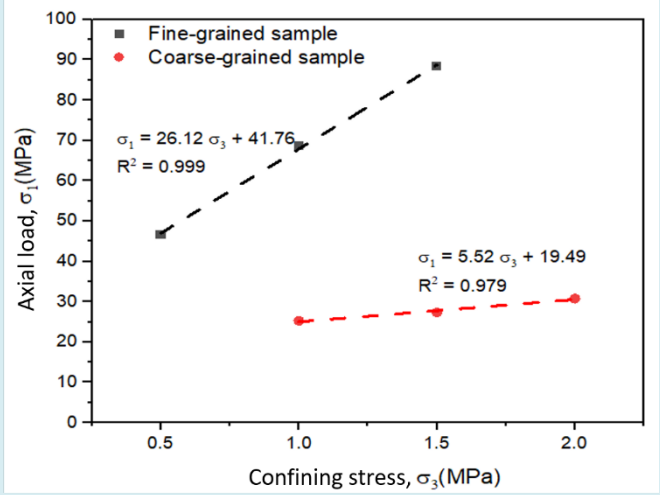



**Figure 16:** Axial load ($\sigma_1$) vs. confining stress ($\sigma_3$) for FG and CG core plugs.

Since there was no provision to measure the lateral strain in the UCS experiments, an empirical relation for intact rock masses [33] as described in Equation 13 was used to calculate the Poisson ratio (Table 7). UCS values in the table are from unconfined (uniaxial) tests and therefore, lower than that estimated from multiple triaxial test curve fitting. Table 7 shows other input parameters for calculating the failure functions provided in Equation 5, 9, and Tables 2, 3.

$$v = 0.25\left(1 + e^{-\frac{UCS}{4}}\right) \quad (13)$$

where, = Poisson's ratio

| S. No | Parameter | Coarse-grained sandstone | Fine-grained sandstone |
|---|---|---|---|
| 1 | UCS (MPa) | 11.50 | 25.45 |
| 2 | Poisson Ratio, v | 0.26 | 0.25 |
| 3 | H-B Parameter, m | 20 | 20 |
| 4 | H-B Parameter, s | 1 | 1 |

**Table 7:** Input parameters for calculating failure functions.

### Failure Envelopes and their Application to $Smp_{wf}$ Determination

Mohr's circles were utilized to estimate the internal friction angle and cohesion from the triaxial tests. Figure 17 shows that the friction angle for CG samples is ~37.5 degrees. Figure 18 shows that the internal friction angle of the FG sample obtained from Mohr's circles is on the higher end (~65 degrees). The cohesion value is dependent on factors, such as mineral composition, water content, bonding agents, and others [34]. It is in the range of 4 to 4.5 MPa for both CG and FG samples.

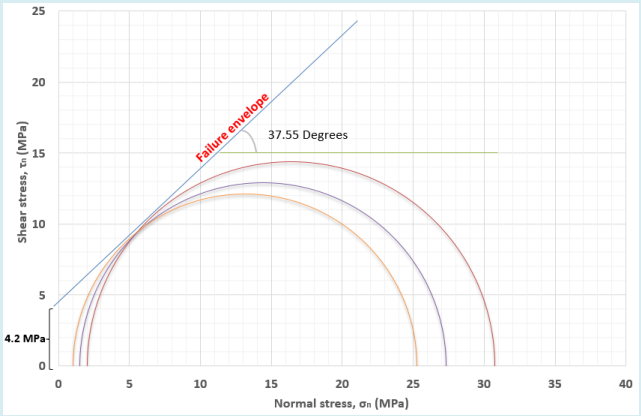



**Figure 17:** Failure envelope for CG samples.

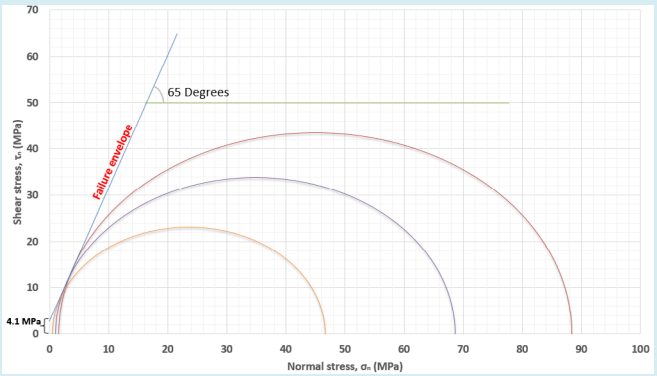



**Figure 18:** Failure envelope for FG samples.

## Discussion

### Evaluation of Failure Criteria

Entering the friction angle and cohesion from the triaxial tests into the three failure criteria (Equation 3 to 6), we obtained predictions on sample failure through the triaxial tests (Table 8). From the quantitative estimation, the D-P criterion predicts that rocks do not fail at the observed failure stresses, even though the rocks failed (Figures 10-15) at the failure stresses, i.e., peak values of $\sigma_1$ (Figures 17, 18). For the D-P criterion, the failure function value 'F' (using Equation 6) ranges between 2.83 and 21.21, which are all



Copyright© Madem VK, et al.

positive, indicating no failure. Part of this situation may arise from considering $\sigma_1=\sigma_2$, due to the limitation of triaxial testing equipment. On the other hand, the M-C and H-B criteria predict rock failure (negative or zero F values) at the observed failure stresses. The F value for the M-C criterion ranges between 0 and -1.45 (using Equation 3), and that for the H-B criterion between 0 and -2.77 (using Equation 5). Therefore, the D-P criterion was deemed unsuitable for predicting the onset of sand production. Further analyses were carried out using M-C and H-B criteria.

| Core Name | Failure Criteria | Result |
|---|---|---|
| TX-CG 1,2,3 | M-C | Rock fails (sand production predicted) |
| TX-CG 1,2,3 | D-P | Rock does not fail (no sand production predicted) (Note: $\sigma_2=\sigma_3$= confining stress was used in the calculation) |
| TX-CG 1,2,3 | H-B | Rock fails (sand production predicted) |
| TX-FG 1,2,3 | M-C | Rock fails (sand production predicted) |
| TX-FG 1,2,3 | D-P | Rock does not fail (no sand production predicted) (Note: $\sigma_2=\sigma_3$= confining stress was used in the calculation) |
| TX-FG 1,2,3 | H-B | Rock fails (sand production predicted) |

**Table 8:** Results of rock failure using the three failure criteria.

### Lower Limit of Flowing Bottomhole Pressure ($SMP_{wf}$) and Critical Drawdown Pressure (CDP) Profiles for FG Samples

Equations in Table 2 and 3 were used to estimate the lower limit flowing bottomhole pressure ($SMP_{wf}$ for sand production using M-C and H-B failure criteria. Figure 19 enumerates the profiles of $SMP_{wf}$ at depth ranging from 147 m – 3000 m for fine-grained samples. The behavior of perforations made at 0-degree azimuth (SHmax direction) and 90-degree azimuth (Shmin direction) were considered. Also, the behavior of perforations created at other azimuths would intercede these two extremes.

At shallow depths (<1 km) the $SMP_{wf}$ values are negative or close to zero for all stress regimes and perforation orientations, indicating minimal chances of sanding (Figures 19 a-f). In a SS regime and depths > 1 km, perforation orientation can make a noticeable difference in sand production. This behavior is indicated by the increasing separation between the lines with depth (Figure 19 c,f). Perforations made in 0 degrees azimuth (SHmax direction) are preferable due to lower $SMP_{wf}$ values. In the SS regime, the M-C criterion provides a more conservative estimate, i.e., higher $SMP_{wf}$ values (by 10-50 MPa), compared to the H-B criterion. Understandably, $SMP_{wf}$ values are lower in the NF compared to the SS regime on average because the NF regime involves lower tectonic compression.

The CDP (difference between the normal pore pressure and $SMP_{wf}$ at a given depth) is a limiting drawdown pressure. If the current drawdown at which the well produces fluids is above the CDP, sand production is predicted. For NF and NF-SS regimes (Figures 20a, b, d, e), at the depth of 147 m, the CDP value at 0 degrees azimuth ($SH_{max}$ direction) is at least 100 MPa higher than the CDP value of perforation at 90-degree azimuth (Shmin direction). However, at greater depths, i.e., > 1 km, sand production is expected in all cases of production because CDP values are either negative or very close to zero (Figure 20 a to f). These results agree with those of Esihet, et al. [35], whose computational simulations indicated that for the same rock, sand production tendency increases with perforation depth.

At any given depth, production in the SS regime has higher chances of accompanying sand production because it has higher stress anisotropy compared to the NF regime. While in an NF regime, the $\sigma_3$ (Shmin) and $\sigma_2$ (SHmax) act on the wellbore cross section, in a SS regime $\sigma_3$ (Shmin) and $\sigma 1$ ($SH_{max}$) act on the vertical wellbore cross section. The difference between $\sigma_3$ and $\sigma_1$ is much higher compared to $\sigma_3$ and $\sigma_2$ at any given depth. As mentioned in Table 4, for the NF regime Shmin gradient = 0.6 psi/ft and SHmax gradient = 0.85 psi/ft, resulting a difference of 0.15 psi/ft. On the other hand, for a SS regime, the Shmin gradient = 0.75 psi/ft and $SH_{max}$ gradient = 1.5 psi/ft, resulting in a difference of 0.75 psi/ft, which translates to a stress anisotropy of 2460 psi (17 MPa) at 3280 ft (1000 m) and 4920 psi (34 MPa) at 6560 ft (2000 m). The reason for no sand production at 147 m depth may also be attributed to the low magnitude of stress anisotropy at shallow depths, which minimizes the chances of perforation failure regardless of the stress regime.



Copyright© Madem VK, et al.

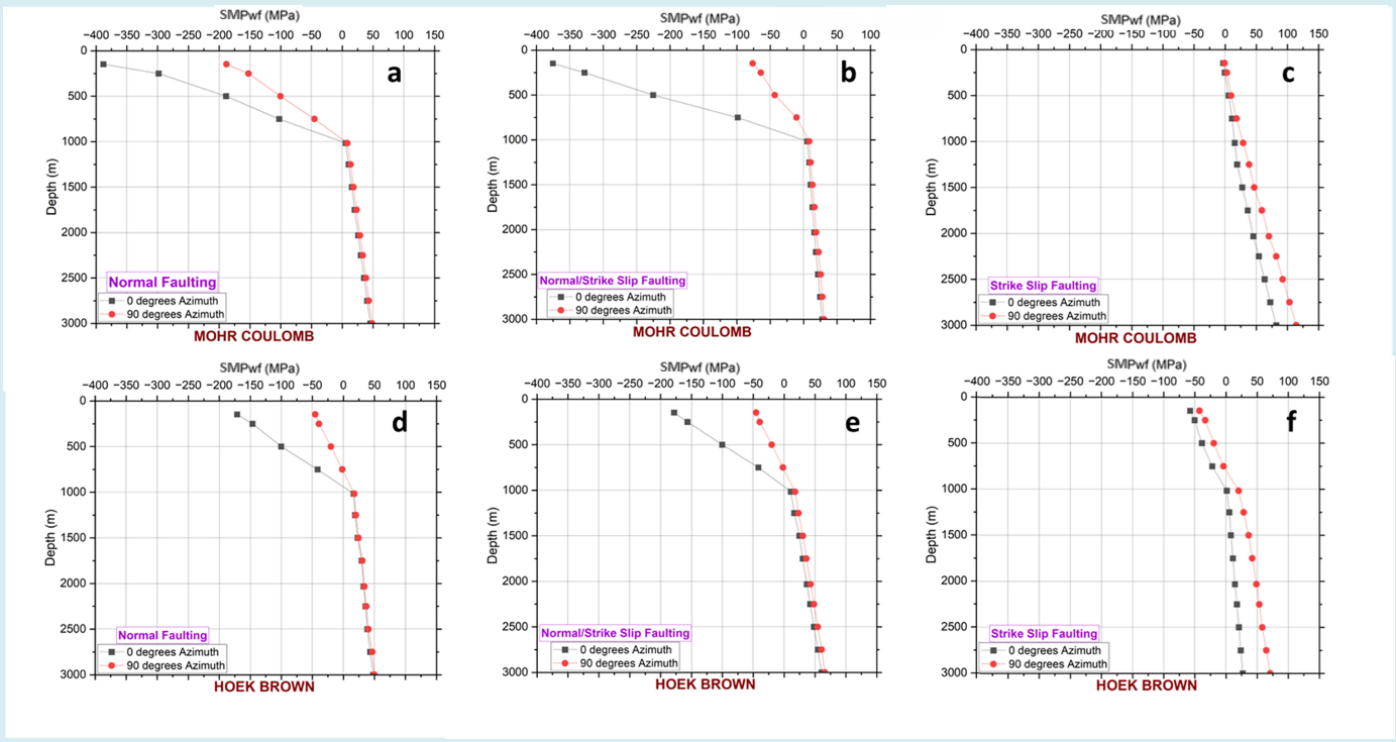



**Figure 19:** Lower limit $SMP_{wf}$ profiles for FG samples assuming normal reservoir pressure.

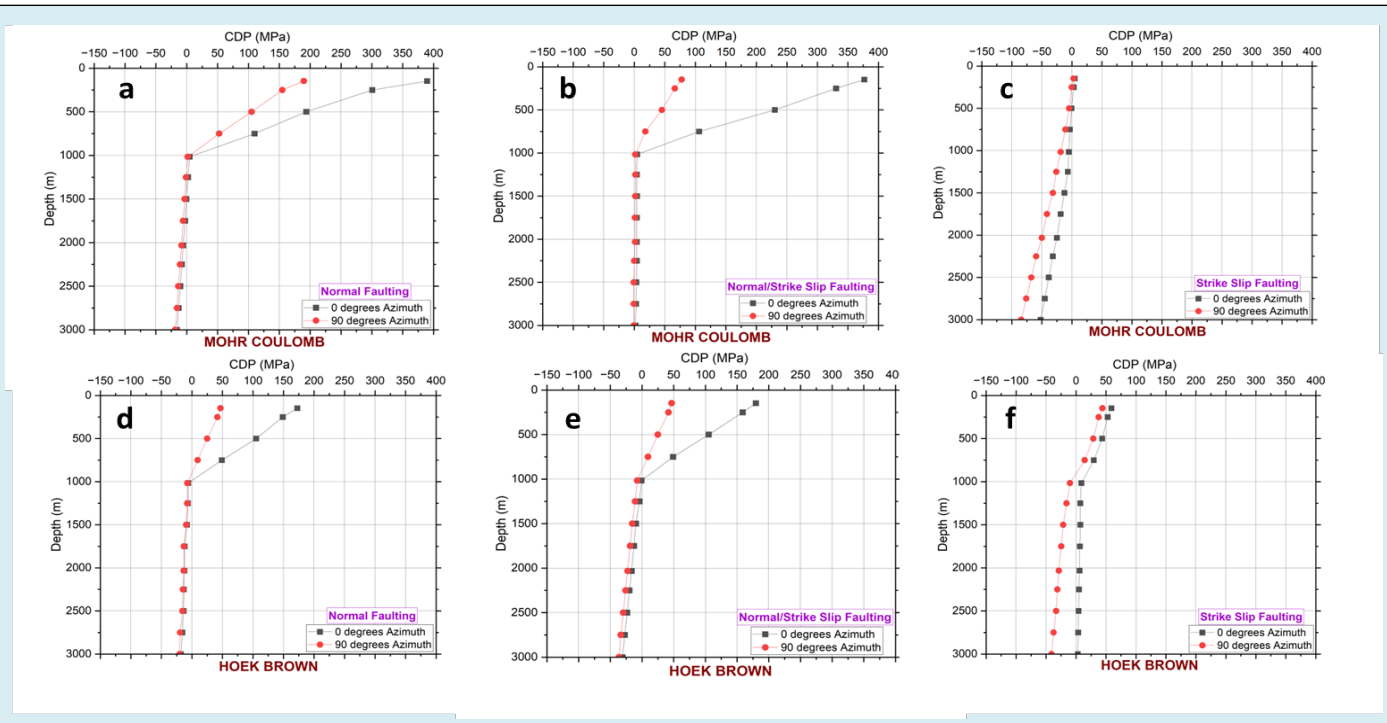



**Figure 20:** Critical drawdown pressure (CDP) profiles for FG samples assuming normal reservoir pressure.



Copyright© Madem VK, et al.

### Lower Limit of Flowing Bottomhole Pressure ($Smp_{wf}$) and Critical Drawdown Pressure (CDP) Profiles for CG Samples

The $SMP_{wf}$ profiles for CG and FG samples are similar, except that CDP values are somewhat lower for CG samples (i.e., higher likelihood of sanding) compared to FG samples due to the lower mechanical strength of CG samples. As shown in Figure 21 (a, b, d, e, f) using either M-C or H-B criteria, at near-surface depths (147 m), regardless of stress regime and perforation direction, the $SMP_{wf}$ values are negative. This observation indicates that sanding would not occur because the theoretical minimum $SMP_{wf}$ possible in an oil well is 0 MPa. Additionally, it is notable that the separation in $SMP_{wf}$ between the two perforation directions is twice in the M-C criterion, compared to the H-B criterion in the NF and NF-SS regimes at near-surface (shallow) depths (Figure 21 a, b, d, e). As observed for FG samples (discussed earlier), this separation is lower at shallow depths in case of the SS regime (Fig 21 c, f). However, at depths > 1 km, the lower limit of $SMP_{wf}$ is above zero in all cases (Figures 21 a-f) and CDP is near or below zero (Figures 22 a-f), indicating chances of sand production regardless of the production rate, perforation direction, and stress regime. Zero CDP values indicate that sand production cannot be contained at any flow rate. These observations agree with those made in Figures 20 and 22 for depths > 1 km. These observations are reasonable, given the increasing difference between the rock strength and principal stress at depth. Tronvoll, et al. [12] reported several near-zero CDP values from 1000-4000 m depth, supporting these observations.

Above-zero CDP at shallow depth (147 m) was observed in all cases (Figures 22 a-f) indicating minimal probability of sand production. A safer bet for perforation stability at depth is to perforate in the SHmax (0 degrees) azimuth because the CDP is almost always higher, or equal at worst, compared to perforation in the Shmin azimuth. A higher CDP is desirable for avoiding sand production. The observation that drilling in the direction of major stress is more stable was also confirmed by Morita and McLeod [36]. The reason for such behavior is that breakouts in vertical wellbores generally occur in the Shmin direction, and perforating in that direction leads to exposure of the perforations to an already stressed and highly compressive wellbore azimuth [10].

Notably, the differences in the perforation stability based on perforation direction (using both H-B and M-C criteria) diminish with depth in the NF and NF-SS regime (Figures 21a, b,d,e and 22 a,b,d,e). In the SS regime, the difference increases by a small margin with depth as evident from the gradually increasing separation between the two curves (Figures 21c, f and 22c, f).

Finally, the onset of sand production estimates presented in this study are conservative because the lower limit of UCS values, based on direct UCS tests, were used for the analysis. “Conservative estimate” means the results indicate a greater likelihood of sand production onset than what may be observed during production. The fact that the anisotropic strength of sandstone was not considered, which is reasonable for massive sandstones, is unlikely to significantly affect these interpretations.

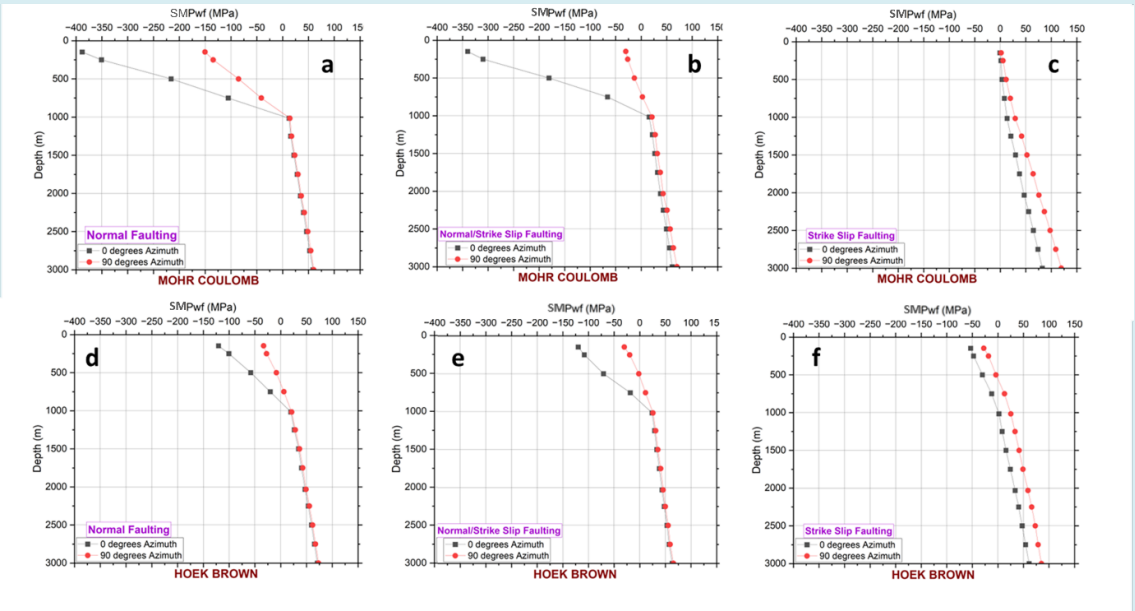



**Figure 21:** $SMP_{wf}$ profiles for CG samples assuming normal reservoir pressure.



Copyright© Madem VK, et al.

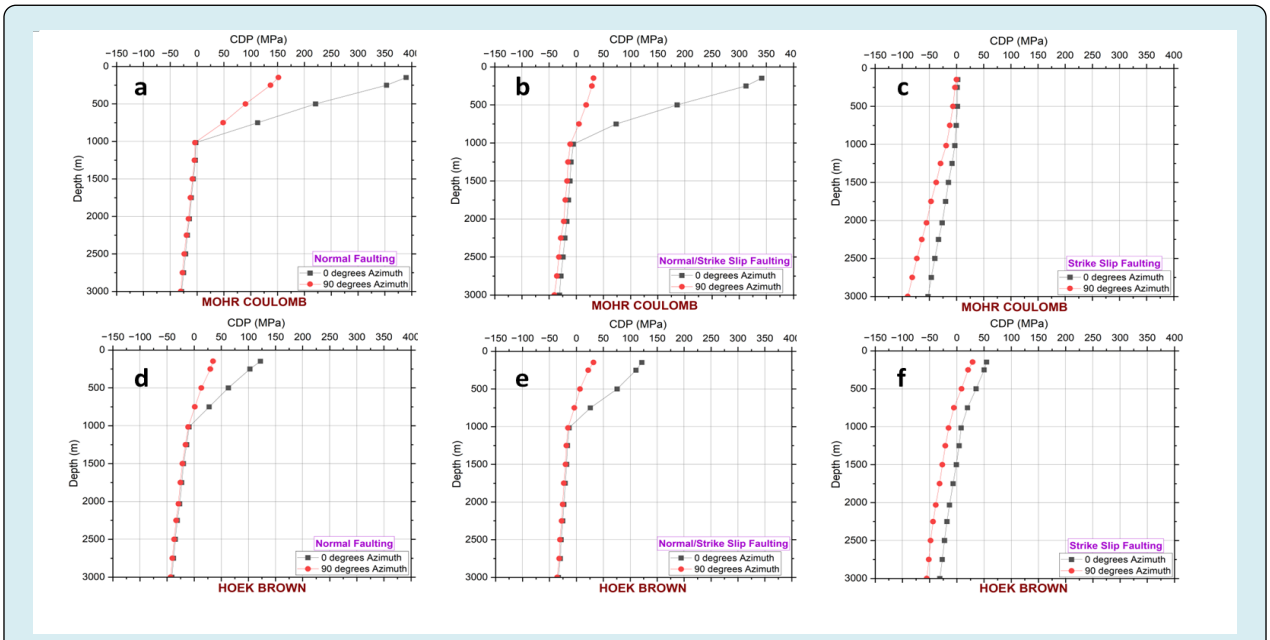



**Figure 22:** Critical drawdown pressure (CDP) profiles for CG samples assuming normal reservoir pressure.

Some observations were made on the effect of different reservoir parameters on the $SMP_{wf}$. For example, an increase in the values of UCS and friction angle allows for lower $SMP_{wf}$. This is probably because higher UCS and friction angle strengthen the rock. Poisson's ratio has an ambiguous relationship with Pwf that depends on the mathematical equation used to calculate SMPwf. CDP has an inversely proportional relationship with SMPwf in all cases because CDP = Pore pressure – SMPwf. In other words, the higher the $SMP_{wf}$, the lower the CDP, and vice-versa.

Regarding the laboratory tests in this work, core plug sample availability and lack of equipment for testing under in-situ conditions of temperature and pore pressure are some limitations. The availability of more core plugs would allow using a greater range of confining stresses during the triaxial tests, aiding in the construction of more accurate failure envelopes. Additionally, since both M-C and H-B criteria neglect the intermediate principal stress (σ2), a degree of inaccuracy has been incorporated in the failure predictions. The intermediate principal stress is known to have some strengthening effect [21]. Therefore, our sanding predictions are conservative, i.e., higher drawdown can be applied before sanding initiates. For more accurate results, polyaxial (true triaxial) tests are required. Additionally, failure criteria, such as the D-P may be reevaluated. However, polyaxial rock testing machines are expensive and not commonly available for use. Another limitation of this study is that it is theoretical, i.e., it does not consider minor changes in rock mechanical properties, if a rock were to be placed at variable depths. Moreover, normal fluid and stress gradients were considered in this study. However, hydrocarbon production from normally pressured reservoirs is not an uncommon phenomenon [37,38]. Not unlike this study, most theoretical studies make some assumptions to bring out important trends related to particular variables of interest.

The strength of this study is that it provides guidelines on sand production trends that may be expected while producing from shallow vs large depths. It considers major factors, such as stress regime, perforation orientation, and rock strength through the lenses of various established failure criteria.

An extension of this work could involve incorporating well log data to construct a 1D mechanical earth model or 3D mechanical earth models using data from multiple wells. These models can help build a field-wide model for sand production using sensitivity analysis of several parameters such as reservoir stress, pore pressure, flow rate, and mechanical rock properties. If substantial sand production is predicted, work may be performed on sand control methods on a well-to-well basis. Moreover, a well-to-well or field-wide NPV (net present value) analysis could be performed for the selected sand control methods to calculate the capital & operational expenditures and the profits that an operating company can expect through sandless hydrocarbon production.

## Conclusion

Sanding is one of the more expensive problems in the oil and gas industry. Upon the onset of sand production, mitigation requires substantial capital investment through



Copyright© Madem VK, et al.

methods, such as gravel packing, resin consolidation, screen placement, and frac pack. A suitable method is to predict and prevent sand production when possible. As per our conservative estimates for a rock of given strength, based on two suitable failure criteria (i.e., M-C and H-B) and two extremes of possible perforation directions (i.e., parallel and perpendicular to SHmax), the major findings on sand production are mentioned below:

1. At large depths (>1 km), any drawdown may cause perforation instability (sand production) based on negative CDP values. This observation is especially true for weaker rocks.
2. At shallow depths (<< 1 km), sand production onset is not likely, regardless of perforation azimuth or failure criteria.
3. At large depths (>1 km) the tendency of sand production is higher in case of the SS regime compared to NF or NF-SS regimes.
4. In most cases, perforation stability is higher when perforations are created in the $S_{Hmax}$ direction, as opposed to the $S_{hmin}$ direction.
5. Both coarse-grained and fine-grained samples show similar trends (not exact values) for the onset of sand production. However, the coarse-grained samples are likely to witness an earlier onset of sand production under similar reservoir conditions due to ~50% lower strength (UCS).
6. Both Mohr-Coulomb and Hoek-Brown failure criteria indicate similar sand production trends. The differences in the perforation stability with perforation direction (using both H-B and M-C criteria) diminish with depth in the NF and NF-SS regime.

These results imply that operators need to be especially careful when producing from sandstones at depths greater than 1 km, especially in compressional tectonic regimes. Placing perforations in a stable configuration, followed by judicious control on the flow rates needs to be exercised. Upon the availability of subsurface data, such as logs, minifracs, and hydraulic fracturing, prior geomechanical models should be built to estimate the amount of required control of the hydrocarbon production rate. Operators may even implement sand control measures prior to the initiation of hydrocarbon production if rock and stress conditions similar to the ones described in this study are encountered.

## Nomenclature

| | |
|---|---|
| $\tau$ | = Shear stress (MPa) |
| $\sigma$ | = Normal stress (MPa) |
| $S_0$ | = Cohesive strength |
| $\varphi_f$ | = Internal friction angle |
| UCS | = Unconfined compressive strength (MPa) |
| $\sigma_1$ | = Major principal stress (MPa) |
| $\sigma_2$ | = Intermediate principal stress (MPa) |
| $\sigma_3$ | = Minor principal stress (MPa) |
| $\sigma_r$ | = Wellbore radial stress |
| $\sigma_\theta$ | = Wellbore tangential stress |
| $\sigma_z$ | = Wellbore axial stress |
| $S_{Hmax}$ | = Maximum horizontal stress (MPa) |
| $S_{hmin}$ | = Minimum horizontal stress (MPa) |
| $S_v$ | = Overburden Stress (MPa) |
| $P_p$ | = Pore pressure (MPa) |
| $S_{Hmax,g}$ | = Maximum horizontal stress gradient |
| $S_{hmin,g}$ | = Minimum horizontal stress gradient |
| $S_{v,g}$ | = Vertical stress gradient |
| $P_{p,g}$ | = Pore pressure gradient |
| $\nu$ | = Poisson's ratio |
| m, s | = Hoek-Brown material constants |
| F | = Failure function |
| UC | = Uniformity coefficient |
| SC | = Sorting coefficient |
| q $\varphi_f$ | = A parameter that depends on the friction angle, |
| $SMP_{wf}$ = Safe minimum bottomhole flowing pressure | |
| CDP = Critical drawdown pressure (Pore pressure – $SMP_{wf}$) | |
| FG = Fine-grained | |
| CG = Coarse-grained | |
| H-B = Hoek-Brown | |
| M-C = Mohr-Coulomb | |
| D-P = Drucker-Prager | |
| NF = Normal faulting | |
| NF-SS = Normal faulting to strike-slip faulting | |
| SS = Strike-slip faulting | |

## Declarations

Conflict of interest: The authors declare no competing interests.

## References

1. Eshiet K, Sheng Y (2013) Influence of rock failure behaviour on predictions in sand production problems. Environmental Earth Sciences 70: 1339-1365.



Copyright© Madem VK, et al.

2. Risnes R, Bratli RK, Horsrud P (1982) Sand stresses around a wellbore. Society of Petroleum Engineers Journal 22(6): 883-898.

3. Morita N, Whitfill DL, Fedde OP, Lovik TH (1989) Parametric study of sand-production prediction: Analytical approach. SPE Production Engineering 4(1): 25-33.

4. Kozhagulova A, Minh NH, Zhao Y, Fok SC (2020) Experimental and analytical investigation of sand production in weak formations for multiple well shut-ins. Journal of Petroleum Science and Engineering 195: 107628.

5. Papamichos E, Furui K (2019) Analytical models for sand onset under field conditions. Journal of Petroleum Science and Engineering 172: 171-189.

6. Reyes R, Sipi A (2018) Optimal sand control design and technique selection: A simplified practical guidance tool. Offshore Technology Conference Asia, Paper D032S004R018.

7. Zhang G, Tan Z, Khaksar A, Gui (2017) Real-time sanding assessment for sand-free fluid sampling in weakly consolidated reservoirs, a case study from Bohai Bay, China. SPE/IATMI Asia Pacific Oil & Gas Conference and Exhibition.

8. Fattahpour V, Moosavi M, Mehranpour M (2012) An experimental investigation on the effect of rock strength and perforation size on sand production. Journal of Petroleum Science and Engineering 86: 172-189.

9. Yi X, Valkó PP, Russell JE (2005) Effect of rock strength criterion on the predicted onset of sand production. International Journal of Geomechanics 5(1): 66-73.

10. Zoback MD (2007) Reservoir Geomechanics. Cambridge University Press.

11. Nemati N, Ahangari K, Goshtasbi K (2024) An investigation of the effect of drawdown pressure on sand production in an Iranian oilfield using a hybrid numerical modeling approach. Journal of Petroleum Exploration and Production Technology 14: 1017-1033.

12. Tronvoll J, Papamichos E, Skjaerstein A, Sanfilippo F (1997) Sand production in ultra-weak sandstones: Is sand control absolutely necessary? Latin American and Caribbean Petroleum Engineering Conference, Rio de Janeiro, Brazil.

13. Song R, Zhang P, Tian X, Huang F, Li Z, et al. (2022) Study on critical drawdown pressure of sanding for wellbore of underground gas storage in a depleted gas reservoir. Energies 15(16): 5913.

14. Bhatt NY, Solanki PM, Prakash N, Das N (2016) View of depositional environment of Himmatnagar Sandstone (Lower–Middle Cretaceous): A perspective. The Palaeobotanist 56: 67–84.

15. Pancholi S, Gudendra Singh Negi GS, Agarwal JR, Bera A, Shah M (2020) Experimental and simulation studies for optimization of water–alternating-gas (CO2) flooding for enhanced oil recovery. Petroleum Research 5(3): 227-234.

16. GSMP (Gujarat State Mineral Policy) (2003) Gujarat State Mineral Policy. Government of Gujarat, India.

17. ASTM International (2020) Standard test method for consolidated undrained triaxial compression test for cohesive soils. ASTM D4767-11 (2020).

18. Olawuyi BJ, Asante S (2016) Particle size distribution methods as adopted for different materials. School of Environmental Technology International Conference (SETIC 2016).

19. ASTM International (2017) Standard test methods for particle-size distribution (gradation) of soils using sieve analysis. ASTM D6913/D6913M-17.

20. ASTM International (2023) Standard test methods for compressive strength and elastic moduli of intact rock core specimens under varying states of stress and temperatures. ASTM D7012-23, Method C.

21. Colmenares LB, Zoback MD (2002) A statistical evaluation of intact rock failure criteria constrained by polyaxial test data for five different rocks. International Journal of Rock Mechanics and Mining Sciences 39(6): 695-729.

22. Hoek E, Brown E (1980) Underground Excavations in Rock. CRC Press.

23. Mansourizadeh M, Jamshidian M, Bazargan P, Mohammadzadeh O (2016) Wellbore stability analysis and breakout pressure prediction in vertical and deviated boreholes using failure criteria – A case study. Journal of Petroleum Science and Engineering 145: 482-492.

24. Eberhardt E (2012) The Hoek-Brown failure criterion. Rock Mechanics and Rock Engineering 45: 981-988.

25. Drucker DC, Prager W (1952) Soil mechanics and plastic analysis or limit design. Quarterly of Applied Mathematics 10(2): 157-165.



Copyright© Madem VK, et al.

26. Li X, Shi L, Bai B, Li Q, Xu D, et al. (2012) True-triaxial testing techniques for rocks—State of the art and future perspectives. In: True Triaxial Testing of Rocks.

27. Kirsch JP (1898) Die Rückkehr der Päpste Urban V. und Gregor XI. von Avignon nach Rom: Auszüge aus den Kameralregistern des Vatikanischen Archivs. F. Schöningh.

28. Huang S, Xia K, Dai F (2012) Establishment of a dynamic Mohr-Coulomb failure criterion for rocks. International Journal of Nonlinear Sciences and Numerical Simulation 13(1): 55-60.

29. Anderson EM (1951) The Dynamics of Faulting and Dyke Formation with Applications to Britain. Oliver and Boyd, Edinburgh.

30. Bhattacharyya S, Das BM (2022) Selection of optimum sand control techniques in some sand-producing fields of Assam Arakan Basin. Arabian Journal of Geosciences 15: 338.

31. Friedman GM (1962) On sorting, sorting coefficients, and the lognormality of the grain-size distribution of sandstones. The Journal of Geology 70(6): 737-753.

32. Shahsavari MH, Shakiba M (2022) An experimental insight into the influence of sand grain size distribution on the petrophysical and geomechanical properties of artificially made sandstones. Journal of Petroleum Science and Engineering 215A: 110632.

33. Aydan Ö, Ulusay R, Kawamoto T (1997) Assessment of rock mass strength for underground excavations. International Journal of Rock Mechanics and Mining Sciences 34(3–4): 18.e1.

34. Giwangkara GG, Mohamed A, Nor HM, Mudiyono R (2020) Analysis of internal friction angle and cohesion value for road base materials in a specified gradation. Journal of Advanced Civil and Environmental Engineering 3(2): 58-65.

35. Eshiet K, Yang D, Sheng Y (2019) Computational study of reservoir sand production mechanisms. Geotechnical Research 6(3): 177-204.

36. Morita N, McLeod H (1995) Oriented perforation to prevent casing collapse for highly inclined wells. SPE Drilling and Completion 10(3): 139-145.

37. Ghosh S, Busetti S, Slatt RM (2019) Analysis and prediction of stimulated reservoir volumes through hydraulic fracturing: Examples from western Arkoma Basin. Journal of Petroleum Science and Engineering 182: 106338.

38. Ghosh S, Zargar Z, Bose S, Thakur G (2022) Lessons learned from the integrated multifarious study of a poorly performing yet great quality oil reservoir: An example from Assam Basin, India. Petroleum Science and Technology 40(17): 2101-2122.



Copyright© Madem VK, et al.

## YOUR RESEARCH DESERVES GLOBAL VISIBILITY

• Publish • Discover • Share • Connect

| MEDICAL | CLINICAL | LIFESCIENCES | PHARMA |
|---|---|---|---|
| 90+ OPEN ACCESS JOURNALS | | 400+ RESEARCH TOPICS | |

SUBMIT YOUR RESEARCH
Submit your manuscript through our online submission system.

REPRINTS
If you require a reprint of any article, please contact us.
info@medwinpublishers.com

BECOME A REVIEWER
Share your expertise and contribute to scholarly publishing.

SCAN TO EXPLORE MEDWIN JOURNALS

• Journals • Submit Manuscript • Reviewer Program • Article Tracking

**Our Journals indexed in**

Embase® ELSEVIER | PubMed National Library of Medicine NLM | Crossref | Google Scholar | INDEX COPERNICUS INTERNATIONAL | ISSN INTERNATIONAL STANDARD SERIAL NUMBER INTERNATIONAL CENTRE | ROAD DIRECTORY OF OPEN ACCESS SCHOLARLY RESOURCES | EuroPub | Scilit | WorldCat® | Academic Resource Index ResearchBib | ADVANCED SCIENCE INDEX | INTERNATIONAL Scientific Indexing | ICMJE INTERNATIONAL COMMITTEE of MEDICAL JOURNAL EDITORS



This article published by **Medwin Publishers,** 28475 Witherspoon Dr, Novi, MI 48377, United States, +1-248-247-6042, WhatsApp +1 (248) 275-1133, info@medwinpublishers.com



© 2026, by the Authors. The articles published from this journal are distributed to the public under "**Creative Commons Attribution License**" (https://creativecommons.org/licenses/by/4.0/). Therefore, upon proper citation of the original work, all the articles can be used without any restriction or can be distributed in any medium in any form.